Effect of rotor dimensions and cross magnetisation on L_d and L_q inductances of reluctance synchronous machine with cageless flux barrier rotor

M.J. Kamper
A.F. Volschenk

Indexing terms: Cross magnetisation, Reluctance machine, Synchronous machine

Abstract: The performance of a reluctance synchronous machine in terms of torque and power factor depends on the two-axis inductances L_d and L_q of the machine. A finite-element analysis method is used to determine these inductances for a reluctance machine with a normal cross-laminated rotor with two flux barriers per pole. By varying the rotor dimensions, the change in the difference and ratio of the inductances is examined. The effect of cross magnetisation on the two-axis inductances is investigated by means of finite element analysis and measurements on an actual reluctance synchronous machine with a two flux barrier per pole rotor. The measured torque of the current-controlled reluctance machine drive is also given and compared with calculated results showing the effect of cross magnetisation. Hence, important conclusions are arrived at regarding the rotor design and cross magnetisation effect.

List of symbols

(Current, voltage and flux linkage phasors are expressed in the rotor reference frame.)

I_s = space phasor of stator currents, A
I_d, I_q = steady-state values of d- and q-axis stator current components, A
V_s = space phasor of stator voltages, V
V_d, V_q = steady-state values of d- and q-axis stator voltage components, V
L_d, L_q = d- and q-axis synchronous inductances, H
L_{dm}, L_{qm} = d- and q-axis inductances due to space-fundamental airgap flux, H
L_{sl} = per phase stator leakage inductance, H
R_s = per phase stator resistance, Ω
λ_s = space phasor of stator flux linkages, Wb
λ_m = space phasor of fundamental airgap flux linkage, Wb
λ_d, λ_q = d- and q-axis stator flux linkage components, Wb
λ_{dm}, λ_{qm} = d- and q-axis fundamental airgap flux linkage components, Wb
ω_r = electrical speed of rotor reference frame, rad/s

Paper 1261B (P1), first received 19th August 1993 and in revised form 5th April 1994

M.J. Kamper is with the Department of Electrical and Electronic Engineering, University of Stellenbosch, Stellenbosch, 7600, South Africa

A.F. Volschenk is with the Unit for Electrical Energy, Department of Electrical and Electronic Engineering, University of Stellenbosch, Stellenbosch, 7600, South Africa

1 Introduction

Current research indicates that the vector-controlled reluctance synchronous machine (RSM) with a high saliency rotor has attractive torque per ampere, power factor and efficiency characteristics that closely resemble those of the induction machine [1–4]. Two factors dominate the output performance of the RSM: the stator and rotor design, and the optimum control of the current space phasor with respect to the rotor. This paper focuses on the rotor design of the RSM and its effect on the performance of the machine.

The investigation is focused on a normal transverse-laminated (cross-laminated) rotor with a limited number of punched flux barriers and saturation bridges. This type of structure was chosen rather than the axially laminated structure due to its simple construction and the fact that the rotor can be skewed. The uncertainty about the high-frequency rotor iron losses of the axially laminated rotor was another reason for not using that type of rotor. In recent research Fratta and Vagati [5] show that a limited number of nonmagnetic segments must be used to avoid high rotor iron losses.

Miller [6, 7] and Vagati [8] made important contributions to the design aspects of RSMs with normal laminated flux barrier rotors. Miller and Debbe [6] report on a specially designed single barrier rotor structure that can also accommodate permanent magnets to obtain a hybrid permanent magnet/reluctance machine. A finite-element analysis method is used to determine the two-axis inductances. The approach of Vagati [8] is to derive simple mathematical equations in order to optimise the rotor structure, so enabling them to do an overall (stator and rotor) maximum torque design.

One obviously important aspect to consider in the design of the RSM rotor is the effect of the rotor dimensions on the inductances of the machine. The inductances are important due to the fact that the torque of the RSM is directly related to the difference between the two-axis inductances, while the maximum power factor in turn is dependent on the ratio of the two-axis inductances. With the RSM under vector control, a cageless rotor can be used and the rotor can be designed to obtain the largest difference and ratio of the two-axis inductances of the machine. The aim of the paper is to show clearly, by

means of a finite-element analysis method, the effect of variation in rotor dimensions on the difference and ratio of the inductances. The effect of varying the stator parameters is not investigated. A standard 5.5 kW induction machine stator with a chorded, double-layer winding is used in the analysis and for the actual machine built.

In addition to the effect of the rotor structure on the inductances of the machine, cross magnetisation has a further effect on the inductances of the RSM with rotors having a limited number of flux barriers per pole. Cross magnetisation or cross coupling is a well-known and important effect in both smooth-airgap and salient-pole machines. The magnetic coupling between the fictitious d- and q-axis windings of the machine originates owing to the variable iron saturation which reduces the average flux density and thus the flux per pole. No clear information is available in the literature about the effect of cross magnetisation on the torque and power factor of the RSM using the flux barrier rotor. The cross magnetisation effect is investigated by means of finite-element analysis and measurements on an actual machine. The measured torque of the current-controlled RSM with a flux barrier rotor is also given and compared with calculated results to show the effect of cross magnetisation.

2 Rotor structure and optimisation

The cross-section of the rotor structure investigated is shown in Fig. 1. The stator of Fig. 1*a* is that of a standard 5.5 kW, four-pole induction machine with a sinusoidally distributed double-layer winding. The double barrier per role rotor of Fig. 1*b* has been built and skewed by one stator slot pitch in an attempt to avoid relatively high cogging torques. This rotor structure was chosen according to the proposed rotor structure of Honsinger [9], without any attempt at optimisation, and because of its simplicity. The higher the number of barriers used the weaker and more pliable the lamination becomes and thus the more difficult to handle. Flux barriers in this paper are defined as the air openings within the rotor iron, although the cut-outs also act as flux barriers. The performance of the reluctance machine under vector control using the rotor of Fig. 1 is outlined in the paper of Kamper and Trübenbach [4]. The torque of this machine equals that of the induction machine counterpart but with the stator current 1.2 times higher, the line voltage 1.1 times lower, and the total copper losses about 30% lower than those of the induction machine. Typical rated data of the RSM of Fig. 1 are

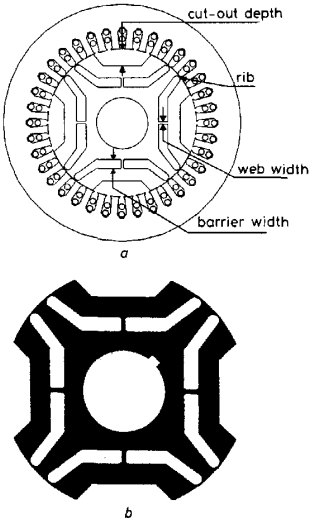

Fig. 1 *Cross-sections of RSM*
a Stator and rotor structures
b Double barrier per pole rotor
Dimensions: Stator outer diameter = 203 mm; rotor outer diameter = 126.3 mm; air-gap length = 0.35 mm; rotor cut-out depth = 14 mm; rotor rib width = 0.7 mm; rotor web width = 2 mm; rotor barrier width (average) = 7 mm; pole-arc = 86° electrical

Line voltage at 50 Hz (full load) = 330 V

Line current (full load) = 15 A

Full load torque = 33 Nm

To study the effect of the change of the rotor structure on the inductances of the machine the following critical rotor dimensions, shown in Fig. 1, are adjusted in the finite-element analysis: flux barrier width, airgap length, web width, and cut-out depth. The rib width of 0.7 mm of the actual rotor is already at a minimum and is not adjusted. Note that as the cut-out depth is varied the pole arc also changes. This is due to the bottom width of the cut-out which stays the same.

2.1 Torque and power factor equations

The equivalent steady-state d- and q-axis circuits of the RSM in the rotor reference frame are shown in Fig. 2.

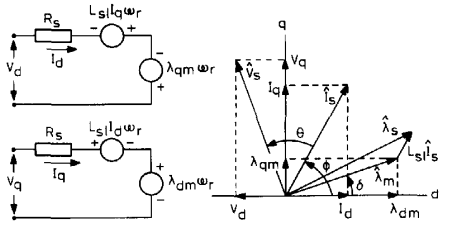

Fig. 2 *Steady-state d- and q-axis equivalent circuits and space phasor diagram of RSM expressed in rotor reference frame*

The core loss resistances are omitted in these circuits. The phasor diagram of the RSM is also shown in Fig. 2. In the phasor diagram the angle θ is the power factor angle, ϕ is the current space phasor angle and δ is the fundamental airgap flux linkage space phasor angle. Inductances L_{dm} and L_{qm} are defined as

$$L_{dm} = \frac{\lambda_{dm}}{I_d}$$

$$L_{qm} = \frac{\lambda_{qm}}{I_q} \tag{1}$$

where

$$\lambda_{dm} = |\lambda_m| \cos \delta$$

$$\lambda_{qm} = |\lambda_m| \sin \delta \tag{2}$$

and

$$I_d = |I_s| \cos \phi$$

$$I_q = |I_s| \sin \phi \tag{3}$$

Inductances L_d and L_q are given by

$$L_d = L_{dm} + L_{sl}$$
$$L_q = L_{qm} + L_{sl} \quad (4)$$

To optimise the design of the RSM rotor, the torque and power factor equations show that the difference and the ratio of the two-axis inductances have to be made as large as possible. The developed torque of the RSM is a direct function of the difference between the d-axis and q-axis inductances L_{dm} and L_{qm} of the machine. The steady-state torque is given by eqn. 5, expressed in the rotor reference frame:

$$T = \tfrac{3}{2}p(L_{dm} - L_{qm})I_d I_q \quad (5)$$

In this equation p is the number of pole pairs. The currents I_d and I_q are under direct current control by using an inverter and control system. The power factor of the RSM in turn is dependent on the ratio of the d-axis to the q-axis inductances L_d and L_q of the machine. By ignoring the stator resistance in the mathematical model of the RSM and by using the phasor diagram of Fig. 2, the power factor of the machine can be written as

$$Pf = \cos\left(\tan^{-1}\left(\frac{\frac{L_d}{L_q}\frac{I_d}{I_q} + \frac{I_q}{I_d}}{\frac{L_d}{L_q} - 1}\right)\right) \quad (6)$$

Hence, two important remarks must be made about eqns. 5 and 6:

(i) The inductance ratio is not and cannot be used as a criterion for the developed torque of the machine, i.e. a high inductance ratio does not necessarily imply a high torque per ampere value for the machine.

(ii) At high inductance ratios (higher than seven) the power factor curve reaches a plateau, i.e. a large change in the inductance ratio is necessary for a considerable change in the power factor. Eqn. 6 shows, for example, that with a 100% increase in inductance ratio (from 7 to 14) the power factor increases by only 18% with $I_q/I_d = 3.7$ (current angle = 75°) and 9% with $I_q/I_d = 1$ (current angle = 45°).

3 Calculation of inductances

The synchronous inductances L_d and L_q of the RSM are calculated by means of a 2-D finite-element analysis program. First the d- and q-axis flux linkages of eqn. 2 are determined. For given d- and q-axis currents I_d and I_q, the amplitude of the fundamental airgap flux density $\hat{B}$ is determined by a Fourier expansion of the radial component of the airgap flux density. The phase angle δ of the fundamental airgap flux phasor is also determined. Eqn. 7 is then used to calculate the amplitude of the fundamental airgap flux linkage space phasor:

$$|\lambda_m| = \frac{2}{\pi}\hat{B}\tau_p l N k_w \quad (7)$$

In this equation τ_p is the pole pitch, l is the effective core length, N is the number of turns in series per phase and k_w is the winding factor. With $|\lambda_m|$, δ and the d- and q-axis currents known, the inductances L_{dm} and L_{qm} are calculated by means of eqns. 1 and 2. The stator leakage inductance L_{sl} is obtained from measurements on the actual three-phase stator winding of the RSM with the rotor removed from the machine. This inductance is measured as $L_{sl} = 4.89$ mH. With L_{sl} known, the inductances L_d and L_q are calculated according to eqn. 4.

Due allowance is made for saturation by using the correct B–H curve of the machine steel in the finite-element program. The effect of skew is also accounted for in the 2-D finite-element analysis by using a technique proposed by, among others, Volschenk [10] and Alhamadi and Demardash [11]. In this way, the core of the machine is axially divided into a number of iron cross-sections or submachines of which the rotors are each skewed a certain angle that is a fraction of the stator slot pitch. With k submachines, each submachine has a core length of l/k, where l is the effective core length of the machine. For each nth submachine the amplitude $|\lambda_m(n)|$ as well as the space angle $\delta(n)$ of the fundamental flux linkage space phasor is determined. The resultant d- and q-axis fundamental airgap flux linkage components are then calculated by means of eqn. 8. In this equation, k is the number of submachines and is taken as $k = 5$ throughout in the analysis. Again, eqns. 1 and 4 are used to calculate the d- and q-axis inductances of the machine. Finally, note that the calculation of the inductances according to the method described does include the effect of cross magnetisation.

$$\lambda_{dm} = \sum_{n=1}^{k} |\lambda_m(n)| \cos \delta(n)$$
$$\lambda_{qm} = \sum_{n=1}^{k} |\lambda_m(n)| \sin \delta(n) \quad (8)$$

4 Analytical results

The rotor of Fig. 1 is analysed by adjusting the flux barrier width, airgap length, web width and cut-out depth. The analysis is done at the condition where the toruqe per current of the machine is a maximum. It is found that for all the different rotor dimensions the torque per RMS current reaches a maximum at a current space phasor angle of close to 60°. Therefore, in all the finite-element computations the current angle ϕ is set to $\phi = 60°$. The RMS stator current is taken as 14.2 A in the analysis, which is close to the rated stator current of the machine. Hence, the d- and q-axis stator currents of eqn. 3 are $I_d = 10$ A and $I_q = 17.4$ A.

4.1 Effect of flux barrier width

The effect of the flux barrier width on the inductances of the machine, keeping the other rotor dimensions constant, is shown in Fig. 3. It can be seen that the optimum

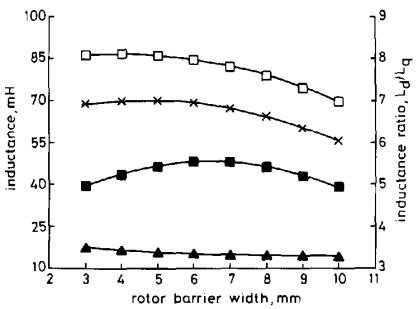

Fig. 3 *Effect of flux barrier width on inductances of RSM*
$I_d = 10$ A; $I_q = 17.4$ A; actual barrier width = 7.0 mm
□—□ L_d ■—■ L_d/L_q
×—× $L_d - L_q$ ▲—▲ L_q

width for the highest inductance ratio is 6.5 mm while the optimum width for the largest difference in the inductances is 4.5 mm. As a result, a width of (say) 5.5 mm will probably be the best to compromise between the widths for highest ratio and largest difference of the inductances. A change in the flux barrier opening from 7.0 mm, i.e. for the actual rotor, to 5.5 mm will lead to an increase of about 4% in the developed torque of the machine due to the increase in the difference between the inductances. The small change in the inductance ratio will have practically no effect on the power factor as is clear from eqn. 6 and Section 2.1 remark (ii). It is important to note that with this change, the volume of the iron in the rotor as a percentage of the total rotor volume (including the rotor shaft) increases from 64 to 72%.

4.2 Effect of airgap length

The effect of change in the airgap length on the inductances of the machine, while keeping the other rotor dimensions constant, is shown in Fig. 4. The airgap

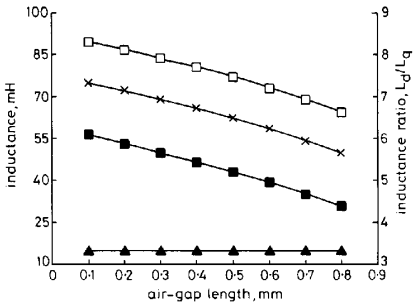

Fig. 4 *Effect of air-gap length on inductances of RSM*
$I_d = 10$ A; $I_q = 17.4$ A; actual air-gap length = 0.35 mm
□—□ L_d
×—× $L_d - L_q$
■—■ L_d/L_q
▲—▲ L_q

length has a considerable effect on the d-axis inductance L_d, but no effect on the q-axis inductance L_q. The fact that L_q does not increase with reducing airgap length is due to the raised cross magnetisation effect of the d-axis flux on L_q (see Section 5). As a consequence, the airgap must be as small as possible for a large inductance difference and a high inductance ratio. There is, however, a mechanical constraint on a minimum airgap length.

4.3 Effect of web width

The effect of the web width on the inductances of the machine is shown in Fig. 5. In reducing the web width from 2.0 (actual rotor) to 0.25 mm the inductance difference and therefore the developed torque show an increase of almost 4%. With this change, the inductance ratio shows an increase of 16% which implies an increase in the power factor of 4.3% according to eqn. 6. The slight reduction of L_d with increasing web width is due to the raised cross magnetisation effect of the q-axis flux on L_d. The graph shows that there is little gain in reducing the web width much below 1.0 mm. A 1.0 mm width, however, plays an important role in the mechanical strength of the lamination. Mechanical breaking strength tests on the rotor lamination of Fig. 1*b* have shown that there is a mechanical safety factor of more than ten with a web width of 1.0 mm at three times base speed (4500 rev/min).

4.4 Effect of cut-out depth

By varying the cut-out depth dimension, the cut-out area and the pole arc of the lamination of Fig. 1*b* are in effect varied. The effect of the change in the cut-out depth on the inductances of the RSM is shown in Fig. 6. The

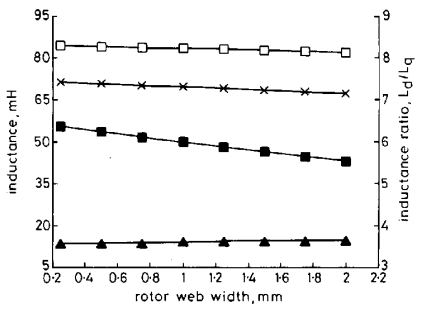

Fig. 5 *Effect of web width on inductances of RSM*
$I_d = 10$ A; $I_q = 17.4$ A; actual web width = 2.0 mm
□—□ L_d
×—× $L_d - L_q$
■—■ L_d/L_q
▲—▲ L_q

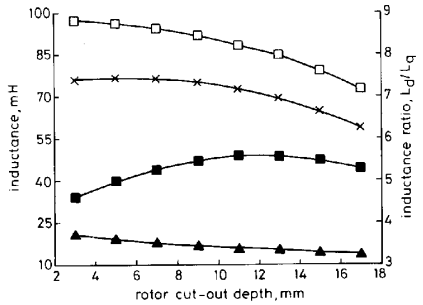

Fig. 6 *Effect of cut-out depth on inductances of RSM*
$I_d = 10$ A; $I_q = 17.4$ A; actual cut-out depth = 14.0 mm
□—□ L_d
×—× $L_d - L_q$
■—■ L_d/L_q
▲—▲ L_q

inductance difference is a maximum at a cut-out depth of 5.0 mm (pole arc = 114° electrical), which is a 15.4% increase from the actual cut-out depth of 14 mm. At this point the percentage rotor iron is 77%. This dramatic increase is due to the large increase in L_d owing to the greater amount of iron used. The inductance ratio in turn reaches a maximum with less rotor iron at a cut-out depth of 12 mm, which is close to the cut-out depth of the actual rotor.

4.5 Optimum barrier width and cut-out depth dimensions

Both the web width and airgap dimensions of the rotor are restricted to certain minimum lengths owing to mechanical constraints. Ideally, the web width of the rotor should be as thin as possible and is reduced in the analysis to a minimum of 1.0 mm (Section 4.3). The airgap cannot be reduced to much less than 0.35 mm for a better torque output. The airgap length is therefore kept at 0.35 mm in the analysis. The other two dimen-

sions, namely barrier width and cut-out depth, can be adjusted without any limit to their optimum values for maximum torque or maximum power factor. The calculated results of this optimisation are shown in Figs. 7 and

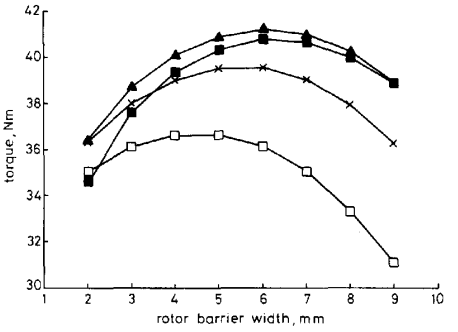

Fig. 7 *Effect of barrier width on torque of RSM with cut-out depth as parameter*

I_d = 10 A; I_q = 17.4 A; web width = 1.0 mm, air-gap length = 0.35 mm
■—■ 3 mm ×—× 11 mm
▲—▲ 7 mm □—□ cut-out = 15 mm

8, respectively, for torque using eqn. 5, and power factor using eqn. 6. With the optimum dimensions for maximum torque (barrier width = 6 mm, cut-out depth = 7 mm), Fig. 7 shows that the developed torque of the machine improves by 17.4% from 35 Nm (actual rotor of Fig. 1*b*) to 41.1 Nm with the same RMS current flowing in the machine. This indicates a dramatic increase in the available torque if optimum rotor dimensions are used. The power factor (Fig. 8) shows an

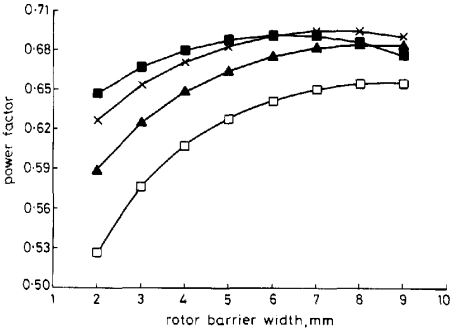

Fig. 8 *Effect of barrier width on power factor of RSM with cut-out depth as parameter*

I_d = 10 A; I_q = 17.4 A; web width = 1.0 mm, air-gap length = 0.35 mm
■—■ 15 mm
×—× 11 mm
▲—▲ 7 mm
□—□ cut-out = 3 mm

improvement of only 3% with optimum dimensions for the barrier width (7.5 mm) and cut-out depth (11 mm). The dimensions of the rotor structure of Fig. 1*b* are thus close to the optimum for highest power factor.

5 Cross magnetisation effect with two flux barrier per pole rotor

A number of studies have been done on the cross-magnetisation effect in reluctance machines [12–14]. These studies have been done on reluctance machines with rotor cage windings without rotor flux barriers. Little is published on the cross magnetisation effect in reluctance machines with axially laminated rotors, but it is shown that the effect with these rotors is low [15, 16].

5.1 Measurement of cross magnetisation

The aim here is to show by means of measurements the effect of cross magnetisation on the inductances of the RSM with the cageless, two flux barrier per pole rotor of Fig. 1*b*. The inductances are measured by simple standstill (locked rotor) decay tests. It is assumed in these tests that, with a sinusoidal distributed stator winding used, the effect of the winding MMF harmonics is negligible. The advantage of this measuring method, compared with standstill AC tests or rotating tests, is that core losses are negligible. The method, however, tends to become inaccurate at very low dq currents, and can also not be used if nonsinusoidal space distributed windings are used in the machine.

The measuring set-up is shown in Fig. 9. Here, the phase current $i_a = 0$ and $i_b = -i_c$. At the time the switch

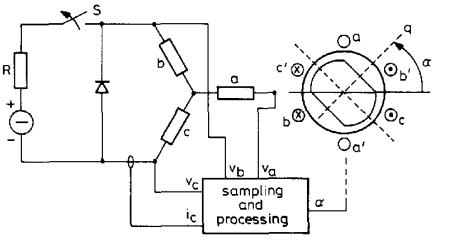

Fig. 9 *Diagram of standstill (locked rotor) measurement of d- and q-axis inductances of RSM to investigate cross magnetisation*

S is opened, the decay phase current and the three phase voltages are monitored. The abc currents and voltages are then transformed to dq quantities by means of Park's transformation. The dq currents and voltages are used in eqn. 9 to determine the instantaneous d- and q-axis stator flux linkage components:

$$\lambda_d = \int_{\infty}^{t} [v_d - i_d R_s]\, dt$$

$$\lambda_q = \int_{\infty}^{t} [v_q - i_q R_s]\, dt \tag{9}$$

Hence, the d- and q-axis synchronous inductances are calculated by

$$L_d = \frac{\lambda_d}{i_d}$$

$$L_q = \frac{\lambda_q}{i_q} \tag{10}$$

It can easily be shown using Park's transformation that for the test set-up of Fig. 9 the dq current ratio is given by

$$\frac{|i_q|}{|i_d|} = \tan \alpha \tag{11}$$

where α is the electrical rotor position but also the current space phasor angle defined in Fig. 2. A number of

decay tests at different rotor positions, and thus different current angles, have been conducted. By using eqn. 9, a series of flux linkage curves $\lambda_d(i_d)$ and $\lambda_q(i_q)$ with the current angle α of eqn. 11 as a parameter have been set up. From these curves, and with careful interpolation, the inductances $L_d(i_d, i_q)$ and $L_q(i_d, i_q)$ are determined using eqn. 10.

The measured results of the cross magnetisation effect on the inductances of the RSM are shown in Figs. 10 and 11. The finite-element analysis results are shown in Figs. 12 and 13. Good agreement is reached between measured

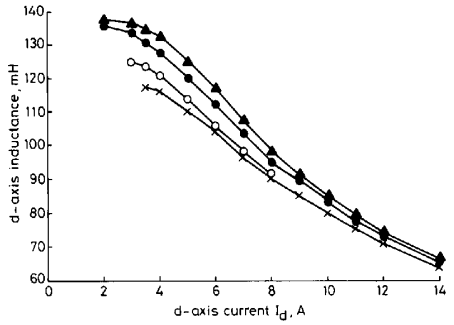

Fig. 10 *Measured effect of cross magnetisation on d-axis inductance of RSM with q-axis current as parameter (rotor of Fig. 1b)*
▲—▲ $I_q = 0$
●—● $I_q = 10$ A
○—○ $I_q = 16$ A
×—× $I_q = 18$ A

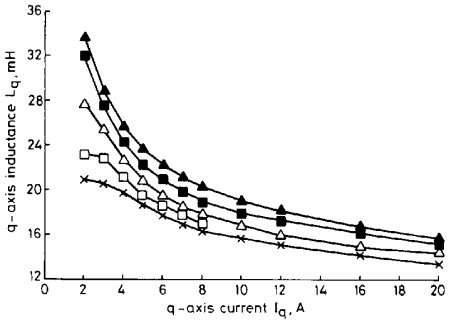

Fig. 11 *Measured effect of cross magnetisation on q-axis inductance of RSM with d-axis current as parameter (rotor of Fig. 1b)*
▲—▲ $I_d = 0$
■—■ $I_d = 3$ A
△—△ $I_d = 6$ A
□—□ $I_d = 8$ A
×—× $I_d = 10$ A

and calculated results which confirms the effect of cross magnetisation. It is clear from these figures that cross magnetisation has a considerable effect on the inductances of the RSM.

5.2 Cross magnetisation effect on inductance difference and inductance ratio

It is important to consider the effect of cross magnetisation on the difference and ratio of the inductances of the machine. This is shown in Fig. 14 for two cases (using the calculated results of Figs. 12 and 13): (i) where the d-axis current is constant with load (Fig. 14*a* and *b*), and (ii) where the current ratio is constant with load (Fig. 14*c* and *d*).

Fig. 14*a* shows that with constant d-axis current the inductance difference and thus the developed torque are increased by 28% at light load but reduced by 7.6% at full-load owing to the effect of cross magnetisation. The cross magnetisation curve in Fig. 14*a* shows that the inductance difference stays constant with q-axis current up to half-load, which implies that in this load region there is a linear relationship between the torque and the q-axis current (eqn. 5). Fig. 14*b* shows that the inductance ratio and thus the power factor are improved throughout by cross magnetisation. The effect of cross magnetisation in Fig. 14*a* and *b* can be explained by the fact that with constant, rated d-axis current, the d-axis inductance is affected slightly (6%) by cross magnetisation (Fig. 12), while the q-axis inductance is greatly reduced particularly at low q-axis currents (Fig. 13). In this respect, constant rated d-axis current control is advantageous.

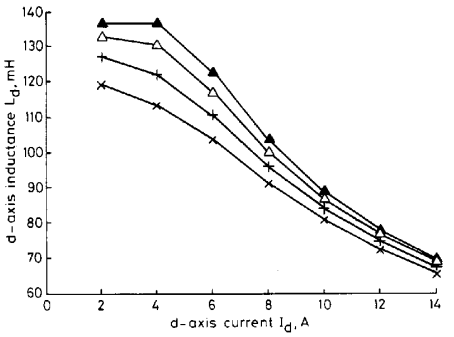

Fig. 12 *Finite-element computations to illustrate effect of cross magnetisation on d-axis inductance of RSM with q-axis current as parameter (rotor of Fig. 1b)*
▲—▲ $I_q = 0$
△—△ $I_q = 6$ A
+—+ $I_q = 12$ A
×—× $I_q = 18$ A

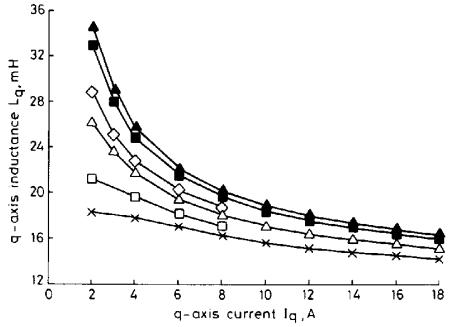

Fig. 13 *Finite-element computations to illustrate effect of cross magnetisation on q-axis inductance of RSM with d-axis current as parameter (rotor of Fig. 1b)*
▲—▲ $I_d = 0$
■—■ $I_d = 3$ A
◇—◇ $I_d = 5$ A
△—△ $I_d = 6$ A
□—□ $I_d = 8$ A
×—× $I_d = 10$ A

Fig. 14*c* and *d* show that, with a high current ratio of $I_q/I_d = 4$, cross magnetisation reduces both the inductance difference and inductance ratio of the machine. The torque is reduced by more than 20% and the power factor by almost 6% at rated q-axis current. This can be explained by the fact that at low d-axis currents, which is the case, the d-axis inductance varies significantly with q-axis current (Fig. 12).

5.3 *Cross magnetisation effect: calculated and measured torque*

The calculated torque with and without cross-magnetisation, using eqn. 5 and the finite-element calculated inductances of Fig. 12 and 13, are shown in Fig. 15. The iron losses are ignored in these calculations. Also shown is the measured shaft torque of the current-controlled RSM drive using the rotor structure of Fig. 1*b*. A GTO VSI and transputer control system are used in the drive. The results show that the effect of cross magnetisation becomes severe at high current ratios (Fig. 15*b*) and as such cannot be ignored in calculations. The difference between the calculated torque with cross magnetisation and the measured torque is due to the iron losses which increase with d- and q-axis current.

6 Conclusions

From the calculated and measured results presented the following conclusions are drawn on the RSM rotor with a limited number of flux barriers per pole:

(i) The rotor of the RSM can either be designed for a high inductance ratio L_d/L_q to obtain a high power factor, or for a large inductance difference $L_d - L_q$ to obtain a high torque per ampere value, or for an optimum between these two.

(ii) With torque a function of the inductance difference $L_d - L_q$ of the RSM and with L_q relatively small, the torque is sensitive to the value of L_d. In all the cases investigated the highest torque is obtained where the L_d value is close to a maximum. For a highly developed torque, the approach in the design must rather be to maximise L_d than to minimise L_q. This leads to a higher percentage of iron used in the rotor.

(iii) With the power factor dependent on the inductance ratio L_d/L_q of the RSM and with L_q relatively small, the power factor is in turn very sensitive to the value of L_q. For a high power factor, L_q must be minimised in the design rather than L_d maximised. This leads to less iron used in the rotor.

(iv) Rib and web widths of the flux barrier rotor must be as thin as possible to minimise L_q, but a speed limit is imposed because of the mechanical strength of the rotor.

(v) The airgap of the RSM should be as small as possible for a high torque output and a high power factor. With rated d-axis current the inductance L_q does not increase with a reducing airgap due to the effect of cross magnetisation.

(vi) With optimum rotor dimensions of the simple double barrier per pole rotor of Fig. 1*b* the torque production of the RSM is greatly improved, making it capable of the same torque production as the squirrel-cage induction machine. Note that with an optimised stator design the performance of the machine may improve even further.

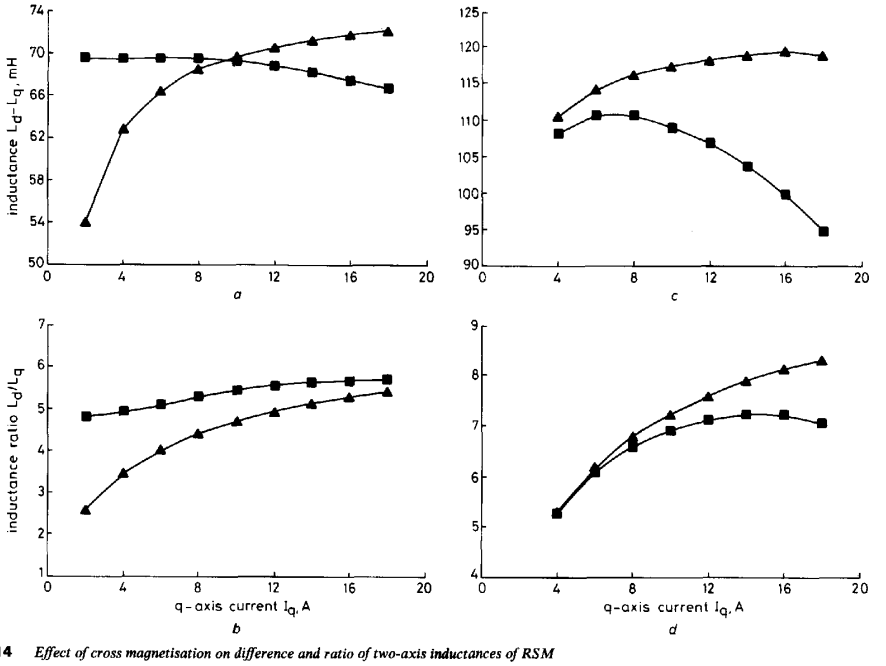

Fig. 14 *Effect of cross magnetisation on difference and ratio of two-axis inductances of RSM*
a and *b* constant d-axis current, $I_d = 10$ A
c and *d* constant current ratio, $I_q/I_d = 4$
■—■ cross magnetisation
▲—▲ no cross magnetisation

(vii) Cross magnetisation has less effect when constant, rated d-axis current control is used.

(viii) With constant, rated d-axis current, the q-axis inductance L_q is greatly reduced by cross magnetisation, particularly at low q-axis currents. This leads to the improvement of the inductance ratio and power factor of the machine.

(ix) Generally cross magnetisation has little effect (5%) on the power factor of the machine.

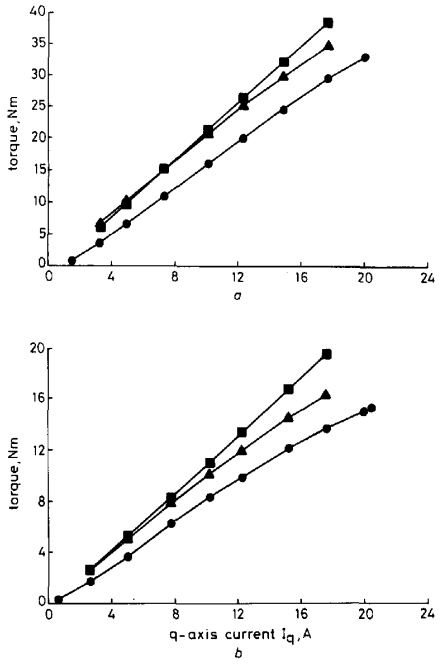

Fig. 15 *Calculated torque (with and without cross magnetisation and measured torque of RSM against q-axis current*

a d-axis current $I_d = 9$ A
b d-axis current $I_d = 3$ A (rotor of Fig. 1*b*; speed = 1000 rev/min)
■—■ no cross magnetisation
▲—▲ cross magnetisation
●—● measured torque

(x) Cross magnetisation greatly reduces the torque of the machine when high two-axis current ratios, i.e. large current space phasor angles, are used.

7 References

1 LIPO, T.A.: 'Synchronous reluctance machines — a viable alternative for AC drives', *Electr. Mach. Power Syst.*, 1991, **19**, pp. 659–671
2 FRATTA, A., and VAGATI, A.: 'Synchronous reluctance versus induction motor: a comparison'. Conference on *Intelligent motion*, 1992, Nürnberg, pp. 179–186
3 BOLDEA, I., FU, Z.X., and NASAR, S.A.: 'Performance evaluation of axially-laminated rotor reluctance synchronous motors'. IEEE IAS Annual Meeting Record, 1992, pp. 212–218
4 KAMPER, M.J., and TRÜBENBACH, T.A.: 'Vector control and performance of a reluctance synchronous machine with a flux barrier rotor'. International conference on *Electrical machines* (ICEM), 1992, Manchester, Vol. 2, pp. 547–551
5 FRATTA, A., VAGATI, A., and VILLATA, F.: 'On the evolution of AC machines for spindle drive applications'. IEEE IAS Annual Meeting Record, 1989, Part 1, pp. 699–704
6 MILLER, T.J.E., and DEBEBE, K.: 'Synchronous reluctance motor design', *Powerconversion Intell. Motion* (USA), 1989, **15**, (8), pp. 73–77
7 MILLER, T.J.E., HUTTON, A., COSSAR, C., and STATON, D.A.: 'Design of a synchronous reluctance motor drive', *IEEE Trans.*, 1991, **IA-27**, (4), pp. 741–749
8 VAGATI, A., FRANCESCHINI, G., MARONGIU, I., and TROGLIA, G.P.: 'Design criteria of high performance synchronous reluctance motors'. IEEE IAS Annual Meeting Record, 1992, pp. 66–73
9 HONSINGER, V.B.: 'The inductances L_d and L_q of reluctance machines', *IEEE Trans.*, 1971, **PAS-90**, (1), pp. 298–304
10 VOLSCHENK, A.F.: 'Finite element analysis of a salient-pole generator feeding a rectifier load'. PhD dissertation, University of Cambridge, 1993
11 ALHAMADI, M.A., and DEMERDASH, N.A.: 'Modelling of effects of skewing of rotor mounted permanent magnets on the performance of brushless DC motors', *IEEE Trans.*, 1991, **EC-6**, (4), pp. 721–729
12 FAUCHER, J., LAJOIE-MAZENC, M., and CHAYEGANI, A.: 'Characterization of a closed-loop controlled current-fed machine taking into account saturation', *IEEE Trans.*, 1979, **IA-15**, (5), pp. 482–484
13 ANVARI, H.A., FAUCHER, J., and TRANNOY, B.: 'An investigation in the influence of a cross-coupling effect on reluctance machine performance'. International conference on *Electrical machines — design and applications*, IEE, 1985, **254**, pp. 70–75
14 BINDER, A.: 'Untersuchung zur magnetischen kopplung von Längs- und Querachse durch sättigung am beispiel der reluktanzmaschine', *Arch. Elektrotech.*, 1989, **72**, pp. 277–282
15 MAYER, R., MOSEBACH, H., SCHRÖDER, U., and WEH, H.: 'Inverter-fed multiphase reluctance machine with reduced armature reaction and improved power density'. International conference on *Electrical machines* (ICEM), 1986, München, part 3, pp. 1138–1141
16 MATSUO, T., and LIPO, T.A.: 'Rotor design optimization of synchronous reluctance machine'. IEEE PES Summer Meeting, Vancouver, 1993, SM 352-5 EC